THE JOURNAL OF PHYSICAL CHEMISTRY C

Article

Cite This: J. Phys. Chem. C XXXX, XXX, XXX−XXX

pubs.acs.org/JPCC

X-ray Absorption and Solid-State NMR Spectroscopy of Fluorinated Proton Conducting Polymers

Z. Blossom Yan,[†] Robin Hayes,[‡] Lis G. A. Melo,[†] Gillian R. Goward,[†] and Adam P. Hitchcock*[,†]

[†]Department of Chemistry and Chemical Biology, McMaster University, Hamilton, Ontario, Canada L8S 4M1

[‡]Department of Physics and Astronomy, The University of British Columbia, Vancouver, British Columbia, Canada V6T 1Z4

Supporting Information

ABSTRACT: ^{19}F and ^{13}C solid-state nuclear magnetic resonance (SSNMR) spectra and near edge X-ray absorption fine structure (NEXAFS) spectra at the S 2p, C 1s, O 1s, and F 1s edges of three different types of perfluorosulfonic acid (PFSA) proton conducting polymers are reported. The NEXAFS spectra were recorded in a scanning transmission X-ray microscope (STXM). They are reported on quantitative intensity scales, suitable for use as reference standards for analytical spectromicroscopy studies. The NEXAFS spectral features are assigned using comparisons to the corresponding spectra of small molecule and polymer analogues, including C 1s and F 1s spectra of polytetrafluoroethylene (PTFE) recorded using STXM. The ^{19}F and ^{13}C SSNMR spectra are reported and analyzed. Within each type of spectroscopy, the spectra of the three types of PFSA are very similar. However, small but statistically significant differences were identified which give insights into how minor molecular structure differences are reflected in the SSNMR and NEXAFS spectra. The relative chemical sensitivity of SSNMR and NEXAFS for studies of PFSA materials is compared. Solution-state NMR diffusion profile analyses of two PFSA ionomer dispersions are also reported.

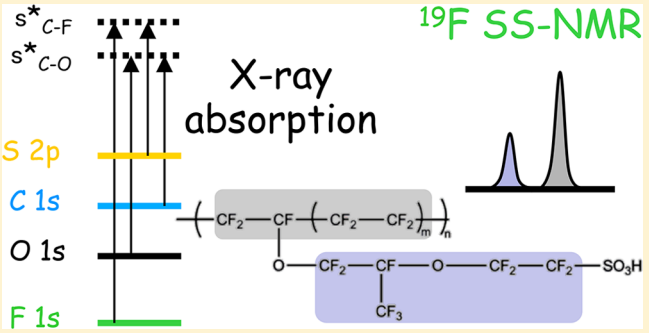

1. INTRODUCTION

Electrochemical conversion of the energy of hydrogen oxidation to useful power has been known for almost two centuries.[1,2] Recent development of efficient perfluorosulfonic acid (PFSA) proton ionic conductors, combined with suitable precious metal catalysts has led to practical, low temperature, proton exchange membrane fuel cell (PEM-FC) systems, which are now used in the aerospace field as auxiliary power sources, commercial stationary power supply applications, as well as mobile power applications in fleet vehicles.[2−4] Many of the major manufacturers of personal automobiles have plans to introduce PEM-FC vehicles, and several manufacturers have products on the market, such as Toyota Mirai and Hyundai Tucson.[5]

Improving fuel cell performance and robustness during operation while reducing use of expensive materials and optimizing manufacturing is a major focus of fuel cell research and development. The physicochemical properties of PFSA materials used in PEM-FC devices as membranes and proton conductors in electrodes (where PFSA is referred to as ionomer) have been investigated intensively in the past several decades. Understanding in detail how the ionomer performance depends on its molecular structure, as well as on how it is distributed in the electrodes, is a route to rational improvement of fuel cell performance and robustness. In PEM-FC devices, hydrogen is oxidized to protons at the anode and oxygen is reduced and combined with protons to form water at the cathode. Both electrochemical reactions are catalyzed. Protons are transported from the anode to the cathode through a proton-conducting, electron-insulating membrane electrolyte, while the electrons generated are passed through an external circuit where they power devices. The proton conductor plays a crucial role in the membrane electrolyte and also in the anode and cathode catalyst layers (CLs). Proton conductor distributions in the cathode are particularly important since the cathode CLs in most PEM-FCs are relatively thick (5−10 μm) and therefore require a system to conduct protons from the electrode-membrane interface to the active catalytic sites throughout the whole thickness.

PFSA is the preferred proton conducting material for both membrane and CL ionomer in current PEM-FCs. PFSA consists of a poly(tetrafluoroethylene) (PTFE or Teflon) backbone and perfluorinated vinyl ether side chains terminated with sulfonic acid groups (see Scheme 1). Nanophase separation of hydrophilic and hydrophobic domains caused by differential hydration of the sulfonated side chains and backbone, provides a dense distribution of sulfonate-rich pockets at the nanoscale[6] which provide pathways for proton transport during fuel cell operation.[3,6−8] Nafion, which is a benchmark PFSA membrane often used in PEM-FCs, is a long-

Received: November 24, 2017
Revised: January 13, 2018
Published: January 16, 2018

DOI: 10.1021/acs.jpcc.7b11592
J. Phys. Chem. C XXXX, XXX, XXX−XXX

Scheme 1. Molecular Structures of the Perfluorosulfonic Acid (PFSA) Ionomer Materials Studied in This Work[a]

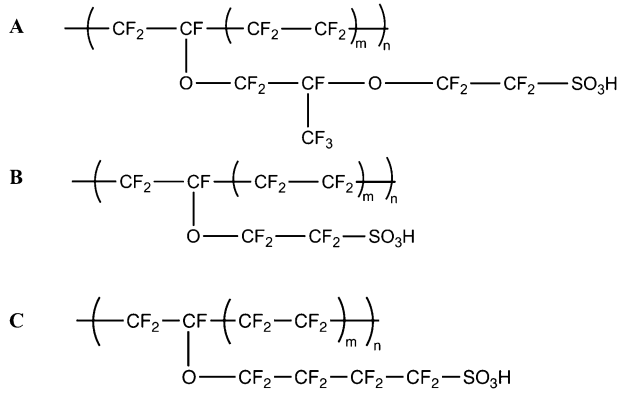

[a](A) Tetrafluoroethylene-perfluoro-3,6-dioxa-4-methyl-7-octenesulfonic acid copolymer (Nafion); (B) tetrafluoroethylene-perfluoro-3-oxa-4-pentenesulfonic acid copolymer (Aquivion); (C) tetrafluoroethylene-perfluoro-3-oxa-4-heptenesulfonic acid copolymer (3M). The value of *m* for each polymer is given in Table 1.

side-chain (LSC) PFSA material where each side chain has two ether groups. Short-side-chain (SSC) analogues with only one ether group, such as Aquivion, are a promising alternative to Nafion. They have been heavily investigated due to their low cost and high ion exchange capacity.[7] Another modification in the side chain of PFSA is a new design introduced by 3M, which is similar to other SSC-PFSA with only one ether group. Examples from these three different types of PFSA materials with different equivalent weight (EW; EW = 100× mass of PFSA per side chain. It is an inverse measure of the relative number of sulfonic acid groups) were measured in the current study (see Scheme 1 for molecular structures and Table 1 for summary of properties). The changes in the side chain structure are meant to reduce the rate of degradation of PFSA by hydroxyl radicals generated during fuel cell operation which mainly attack the ether bond(s) due to their relatively high electrophilicity.[9,10]

Spectroscopies are important tools for material analysis. Maximum benefit from any given spectroscopy is gained when a detailed interpretation of all spectral features can be given. Soft X-ray scanning transmission X-ray microscopy (STXM) has been used to quantitatively map the ionomer, carbon support and catalysts in membrane electrode assemblies (MEAs).[11−19] Analytical transmission electron microscopy based on core level electron energy loss spectroscopy (TEM-EELS) has been applied to PFSA materials.[20,21] STXM has significant advantages relative to TEM-EELS since STXM causes much less radiation damage for similar levels of analytically useful information.[19,22−24]

NMR is a powerful tool to probe the structure of materials. From the perspective of solid-state NMR (SSNMR), a solid material consists of nuclear spins with random orientations. The randomness in spin orientation produces different frequencies in the applied magnetic field, i.e., chemical shifts, due to chemical shielding and dipolar coupling interactions, which leads to line broadening in NMR spectra. The orientation dependence of the chemical shift is referred to as chemical shift anisotropy (CSA). The magic angle spinning (MAS) technique, which involves spinning the sample about an angle of 54.74°, is used in SSNMR.[25,26] By doing so, the orientation-dependent interactions are averaged to zero on the time scale of rotor revolution speed, which mimics molecular tumbling in the solution state. As a result, the CSA and the dipolar coupling interactions are mostly removed and well-resolved solution-state-like spectra are obtained. ^{19}F SSNMR provides exquisite chemical site differentiation averaged over the whole sample. However, ^{13}C and ^{33}S SSNMR are very challenging, due to the low sensitivities associated with low natural isotopic abundances of both nuclei, as well as the low gyromagnetic ratio and large quadrupole moment of ^{33}S. Hence, an integrated method that combines XAS and SSNMR can provide structural information at the molecular level for all of the elements in PFSA. In addition, if XAS is measured in state-of-the-art soft X-ray microscopes, it can provide chemical environment information at the few tens of nanometers spatial scale.[12−16,27,28]

This study has measured the ^{19}F and ^{13}C solid state nuclear magnetic resonance (SSNMR) and C 1s, F 1s, O 1s and S 2p near edge X-ray absorption spectra (NEXAFS) of three different types of PFSA as well as PTFE. The results are used to develop spectral-structure relationships, and to investigate the extent to which these two spectroscopies can provide complementary information about PFSA materials. The combination of NMR and NEXAFS for studies of polymeric materials has been applied to biopolymers.[29] NMR and hard X-ray absorption spectroscopies have been combined to investigate solid heterogeneous polymeric catalyst materials.[30,31] To our knowledge, this is the first report of NMR and NEXAFS spectra applied to the same PFSA materials.

The paper is organized as follows. After describing the experimental procedures, the XAS spectra are presented, with interpretation aided by comparison to small molecule analogs. The ^{19}F NMR spectra are then presented and interpreted. Results of a comparative study of molecular diffusion in two ionomer dispersions are then reported to illustrate another capability of NMR that is important to PEM-FC optimization. The relative sensitivity of NMR and NEXAFS to differences in the molecular structure of the three classes of PFSA is then discussed, including cast films from ionomer dispersions, followed by a short summary.

2. EXPERIMENTAL SECTION

2.1. Materials and Sample Preparation. *2.1.1. Membrane Sample Activation.* Pristine Nafion117 was purchased from Sigma-Aldrich. Aquivion PFSA ionomer membranes were obtained from Solvay, Italy. 3M "new" PFSA ionomer

Table 1. Summary of Properties of the PFSA Membrane Materials Studied in This Work

name	PFSA type	EW[a]	*m*	formula	*M* (g/mol)	density (g/cm^3)	# of C−F	# of C−C	# of C−O
Nafion117	LSC	1100	6.5	$C_{20}F_{39}SO_5H$	444	1.98	39	17	4
Aquivion98	SSC	980	7	$C_{18}F_{35}SO_4H$	278	1.98	35	16	2
3M-725	3M SSC	725	3.5	$C_{13}F_{25}SO_4H$	378	1.98	25	11	2

[a]Reference 61.

DOI: 10.1021/acs.jpcc.7b11592
J. Phys. Chem. C XXXX, XXX, XXX−XXX

membranes[32] were obtained from 3M, St. Paul, MN. The PFSA materials were first washed in 3 wt % H_2O_2 for 1 h at 90 °C and then washed with deionized water for another hour, changing the water every 15 min. Subsequently, they were washed in 0.5 M H_2SO_4 solution for 1 h. They were then washed in deionized water until a constant pH was obtained. Finally, the materials were dried in vacuum oven at 80 °C for 24 h.

2.1.2. Cast Film Preparation. An aqueous dispersion with 60 wt % PTFE was purchased from Sigma-Aldrich. It was diluted to 2 wt % using H_2O (HPLC grade), spin coated onto freshly cleaved mica (1000 rpm/30 s), and annealed at 190 °C for 2 h. Nafion and Liquion alcoholic dispersions (EW = 1100) with 5 wt % were obtained from Ion Power Inc. and diluted with isopropanol into 3 wt % concentrated solutions. These solutions were spin coated (30 s @ 3000 rpm) on to freshly cleaved, 1 cm × 1 cm mica squares. The film covered mica was scored into an array of 1 mm × 1 mm squares. The polymer film was then transferred via a clean surface of deionized water to a silicon nitride window. The film chip on the SiN_x window was vacuum annealed at 70 °C for 2 h, then used for STXM measurements. Some spectra were also measured from ultramicrotomed blocks (see Figure 1) or were recorded from the membrane area of PEM-FC MEAs.

2.1.3. Ionomer Dispersions for NMR Study. For solution-state diffusion study, Nafion and Liquion dispersions (EW = 1100) were obtained from Ion Power Inc. and diluted with *n*-propanol (NPA) aqueous solution with volume ratio NPA/H_2O = 3:1 into 1% concentrated solutions. For SSNMR spectral analyses, the dispersions were cast onto clean Petri dishes at 80 °C under active vacuum for 4 h, then dried overnight.

2.2. X-ray Absorption Spectroscopy. The X-ray absorption spectra were recorded using the STXM microscope[33] on beamline 5.3.2.2[34] at the Advanced Light Source (ALS, Lawrence Berkeley National Laboratory (LBNL), Berkeley, USA), and the ambient STXM on beamline 10ID1[35] at the Canadian Light Source (CLS, Saskatoon, Canada). In STXM a monochromated X-ray beam is focused to a small spot (~30 nm) using a Fresnel zone plate and an order sorting aperture to select only the first order light. The sample is positioned at the X-ray focal spot and X-Y raster scanned under interferometer control while detecting the transmitted X-rays. Further details are given in recent review articles.[27,36,37]

The PFSA samples studied by STXM were prepared using ultramicrotomy at the Department of Pathology and Molecular Medicine at McMaster University. Sections with a nominal 100 nm thickness were prepared for each PFSA sample, and placed on Formvar coated TEM grids. In addition to allowing measurements of areas of near uniform thickness, the transmission detection used in STXM does not suffer from artifacts which can occur with yield based detection like total electron yield or X-ray fluorescence yield. Figure 1a presents a STXM optical density (OD) image of the Nafion117 sample, measured at 200 eV before and 292.6 eV after the spectral measurements. The absence of rectilinear contrast at the area of spectral measurement in Figure 1b verifies the measurements were performed without significant radiation damage. Soft X-rays from 150−780 eV, covering the S 2p, C 1s, O 1s, and F 1s edges, were used. After loading the sample, the STXM chamber was evacuated to a pressure of 0.1 mbar, and then the tank was backfilled with 0.3 bar of He gas. A N_2 gas filter (at ALS 5.3.2.2) or a Ti filter (at CLS 10ID1) was used to block second order light when measuring the C 1s spectra. The spectra were

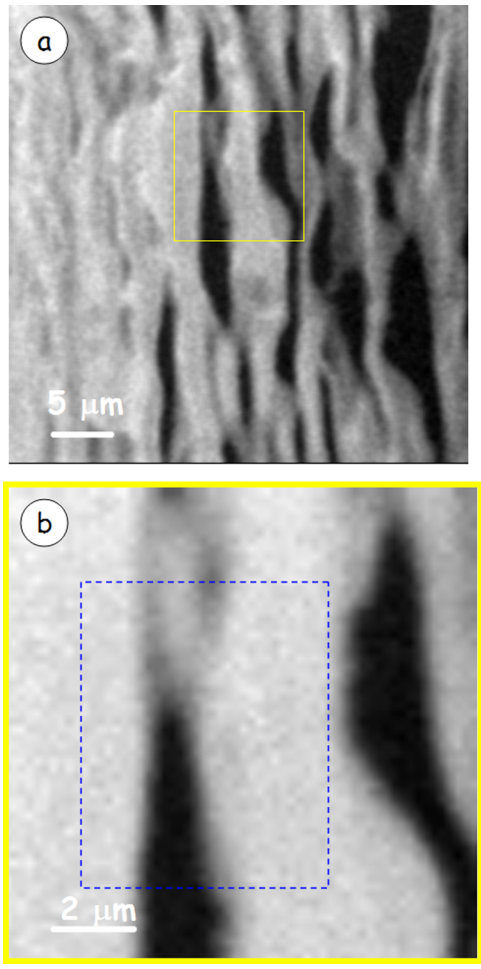

Figure 1. (a) Optical density (OD) image of an ultramicrotomed section of Nafion117 PFSA, recorded with scanning transmission X-ray microscopy (STXM) at 200 eV. The yellow rectangle indicates the region for spectral study (blue rectangle in Figure 1b) which was chosen to include an open area (rip in the microtomed section) to use as an internal I_0. (b) OD image measured at 292.6 eV after measuring stacks at all 4 edges (F 1s, C 1s, O 1s, and S 2p) using a 200 nm defocused beam. The stacks were measured in the area outlined by the blue dashed rectangle. This area was subjected to a total exposure time per pixel of 600 ms.

acquired using image sequences ("stacks"[38]) over a large area, using a defocused beam and a step size the same or larger than the defocused spot size in order to minimize radiation damage, which is a severe problem with PFSA materials.[24] For the C 1s, F 1s, and O 1s edges, a dwell time of 1 ms per pixel was used. For the S 2p edge, where the incident flux is much smaller and the amount of S small, a dwell time of 4 ms per pixel was used. The I_0 was measured simultaneously with the I signal by including an area in the stack with just the Formvar or silicon nitride support (Figure 1). After each stack, an area larger than the stack area was imaged at 292.6 eV where the radiation damage has its strongest effect. If the change in intensity between outside and inside the stack frame was more than 5% the stack was remeasured using a less focused beam. After image alignment, the transmitted I and I_0 signals were combined to generate the optical density (OD, or absorbance) signal from the Lambert−Beer law, OD = $-\ln(I/I_0)$. The spectra reported are the average over all areas with an OD less than 1.2. The C 1s, O 1s, and F 1s spectra were then converted

DOI: 10.1021/acs.jpcc.7b11592
J. Phys. Chem. C XXXX, XXX, XXX−XXX

to an absolute intensity scale, optical density per nanometer (OD1), by scaling to match the pre- and postedge spectral intensities to that predicted for the elemental composition of the material (see Table 1), using X-ray absorption coefficients from the literature.[39] For the S 2p spectra, which have a low signal to background ratio, the underlying non-S 2p signal was subtracted using a spline curve fit to the pre-edge signal in order to properly visualize the S 2p spectral features. All data processing was performed using aXis2000.[40]

2.3. NMR Spectroscopy. The ^{19}F SSNMR spectra of the activated PFSA materials and cast dispersion samples (prepared as described in 2.1) were measured on a Bruker Widebore −300 MHz Avance III system using a double-resonance probe that supports rotors with an outer diameter of 4.0 mm with 15 kHz MAS spinning speed (chemical shift referenced using trichlorofluoromethane, $CFCl_3$, (δ = 0 ppm). All ^{19}F NMR experiments were performed using a pulse at 97.5 kHz radiofrequency (RF) field, with 5 s recycle delay. The solution state diffusion NMR spectroscopy was done using a Diff50 diffusion probehead at variable temperatures ranging from 295 to 350 K. A pulse field gradient stimulated echo (diffSte) pulse sequence was used. This sequence and the associated gradient parameters are described in section A of the Supporting Information. The ^{13}C SSNMR measurements were conducted using a 1.9 mm outer diameter rotor with 40 kHz MAS on a Bruker Ascend 850 MHz system (chemical shift referenced using adamantane, $C_{10}H_{16}$ δ = 38.5 ppm for high-frequency peak). All measurements were performed using an 83.3 kHz RF field, with 15 s recycle delay.

3. RESULTS

3.1. X-ray Absorption Spectra. *3.1.1. C 1s Spectra.* Each peak in an XAS spectrum arises from transitions from the ground state to an inner shell (core) excited state where the core hole is localized on one specific atom.[41] The intensities are determined by the electric dipole transition matrix element. Thus, the spectral features provide information about chemical bonding around that core-excited atom. We focus on peak shapes and energies of the observed features. Detailed assignment of the C 1s, F 1s, O 1s, and S 2p spectra provides links between the spectral features and the chemical structures of the three types of PFSA. The S 2p edge spectrum is sensitive to the side chain in PFSA materials, since that signal arises exclusively from the sulfonic acid groups. This is particularly relevant, as the sulfonic acid site controls the proton conductivity of the membrane.

Figure 2 compares the C 1s spectra of Nafion117, Aquivion98, and 3M-725 PFSA to that of PTFE. Proposed peak assignments are presented in Table 2. The C 1s spectra are dominated by four strong peaks at 292.5, 295.5, 299, and 307.5 eV, which are also seen in other heavily fluorinated saturated[42] and unsaturated fluoro-organic compounds,[43] as well as polymers such as Teflon.[44−46] The peaks at 292.5, 295.5, and 299 eV, correspond to C 1s(CF_2) → σ^*_{C-F} transitions, while those at 295, 307.5, and 326 eV correspond to C 1s(CF_2) → σ^*_{C-C} transitions. From C 1s XAS studies of aligned PTFE[45,46] the peak at 292 eV is associated with C 1s(CF_2) → σ^*_{C-F} (∥) excitations, where the σ^*_{C-F} (∥) orbital is aligned perpendicular to the C−C chain. The peaks at 295 and 299 eV are associated with C 1s(CF_2) → σ^*_{C-F} (⊥) and C 1s(CF_2) → σ^*_{C-C} (⊥) excitations, where σ^*_{C-F} (⊥) and σ^*_{C-C} (⊥) orbitals are aligned along the C−C chain. All three PFSA species have a branch carbon site with two ($-CF_2$), one F and one O attached, while Nafion has a second similar C 1s(CF) site in its side chain. The C 1s level for this site will be ∼1 eV lower in binding energy than the majority C 1s (CF_2) sites which would shift the σ^*_{C-F} and σ^*_{C-C} transitions to lower energy. However, these sites are 1 in ∼14 of the carbons in Aquivion98 and 1 in ∼7 of the carbons in Nafion117 and 3M-725, so these transitions are masked by the much stronger C 1s(CF_2) features. Note this is in sharp contrast to the ^{19}F SSNMR, where signals from each chemically distinct site are detected (section 3.2.1).

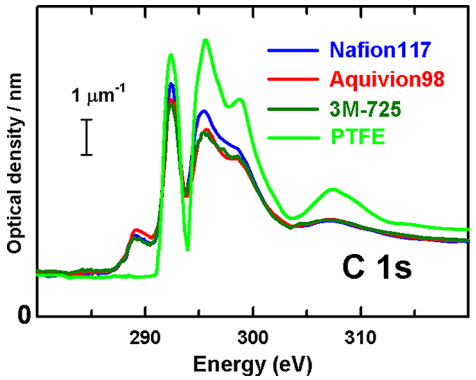

Figure 2. C 1s X-ray absorption spectra of Nafion117, Aquivion98, 3M-725, and polytetrafluoroethylene (PTFE) recorded using STXM. The spectra have been converted to an absolute intensity scale (optical density/nm thickness at standard density, OD1) using the procedures described in the text. Peak positions and tentative assignments are given in Table 2.

In addition to the peaks seen in PTFE, the C 1s spectra of all three PFSA show a structured peak at 289.1 eV. We attribute this striking difference to the presence of oxygen in the PFSA materials. Initially we attributed the 289.1 eV signal to C 1s(CF_2) → σ^*_{C-O} transitions at the ether groups in the side chains. However, C 1s → σ^*_{C-O} features are typically observed at higher energies.[47] At present, we attribute the 289.1 eV peak to C 1s(COOR) → $\pi^*_{C=O}$ transitions at the termination of the −(CF_2)− main chain. For comparison, the C 1s(COOR) → $\pi^*_{C=O}$ transition in CF_3COOH occurs at 288.2 eV.[43] In partial support for this tentative assignment, the ^{13}C SSNMR provides evidence of carbonyl signal (see subsection 3.2.2).

From a comparative point of view, Aquivion98 and Nafion117 have similar EW despite having different side-chain lengths. Nafion117 has more C−C bonds per formula unit compared to Aquivion98, while 3M-725 has the smallest number of C−C bonds per repeating unit. This is consistent with the relative intensities of the transition at 295 eV (Figure 2) which arises primarily from C 1s(CF_2) → σ^*_{C-F} (⊥) and C 1s(CF_2) → σ^*_{C-C} (⊥) excitations, in the main chain.

3.1.2. F 1s Spectra. Figure 3 compares the F 1s spectra of Nafion117, Aquivion98, 3M-725 PFSA with that of PTFE. Detailed transition assignments are presented in Table 3. As with the C 1s spectra, the F 1s spectra of the three PFSA are very similar, with each PFSA having the same F 1s spectral features with very similar intensities. In contrast to the C 1s edge, the F 1s spectra of all three PFSA species are much closer to that of PTFE. The F 1s spectra are dominated by strong F 1s → σ^*_{C-F} peaks at 689.8 and 694.0 eV. By comparison to the F 1s spectra of aligned PTFE[45] the first peak at 689.8 eV is associated with excitations to σ^*_{C-F} (⊥) orbitals oriented across the C−C chain direction while the peaks at 693.4, 704,

DOI: 10.1021/acs.jpcc.7b11592
J. Phys. Chem. C XXXX, XXX, XXX−XXX

Table 2. Summary of Peak Positions and Tentative Assignments for Spectral Features in the C 1s Spectra of PTFE, Nafion117, Aquivion98, and 3M-725

energy (eV)				Assignment	
PTFE	Nafion117	Aquivion98	3M-725	C−O	CF_2
–	287.8 (sh)	287.8 (sh)	287.8 (sh)		
–	289.1	289.2	289.1	σ^*(C−O)	
292.4[a]	292.4[a]	292.5[a]	292.4[a]		σ^*(C−F) ∥
294.8 (sh)	–	–	–		σ^*(C−C)
295.6	295.4	295.7	295.4		σ^*(C−F) ⊥
298.7	298.8	298.6	298.5		σ^*(C−F) ∥
307.6	307.2	307.4	307.2		σ^*(C−C)
326 (br)	326 (br)	326 (br)	326 (br)		σ^*(C−C)

[a]Calibration: PTFE: −2.56 (4) eV; Nafion117: −2.54 (4) eV); Aquivion98: −2.48 (4) eV); 3M-725: −2.46 (4) eV, relative to C 1s → 3p transition of CO_2 (294.96(2)[62]).

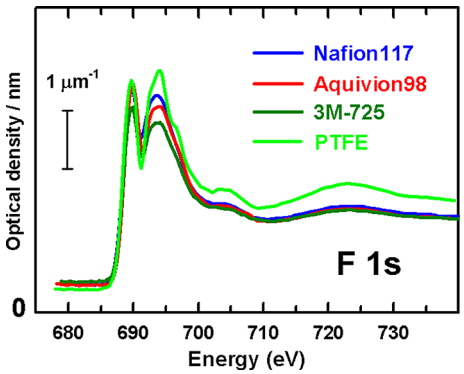

Figure 3. F 1s X-ray absorption spectra of Nafion117, Aquivion98, and 3M-725 recorded using STXM. The spectra have been converted to an absolute intensity scale (optical density/nm thickness at standard density, OD1) using the procedures described in the text. Peak positions and tentative assignments are given in Table 3.

Table 3. Summary of Peak Positions and Tentative Assignments for Spectral Features in the F 1s Spectra of PTFE, Nafion117, Aquivion98, and 3M-725

energy (eV)				assignment
PTFE	Nafion117	Aquivion98	3M-725	CF_2
689.7	689.8	689.9	689.8	σ^*(C−F) ⊥
692.7 (sh)		692.8 (sh)		
694.1[a]	693.8[a]	694.2[a]	693.7[a]	σ^*(C−F) ∥
696.7 (sh)	–	697.1 (sh)	–	
704.1	704.2	704.6	704.3	σ^*(C−F) ∥
723 (br)	723 (br)	723 (br)	723 (br)	σ^*(C−F) ∥

[a]Calibration: PTFE: +5.8(1) eV; Nafion117: +5.5(1) eV; Aquivion98: + 5.9(1) eV; 3M-725: +5.4(1) eV, relative to F 1s → a_{1g} transition of SF_6 (688.27(15)[63]).

and 723 eV are associated with σ^*_{C-F} (∥) orbitals oriented along the C−C chain direction. There are small but reproducible differences in the intensities of the two main F 1s peaks among the three PFSA. Given that the relative intensities of the two main F 1s NEXAFS peaks can change dramatically with molecular orientation,[45] one might suspect that the variations in the spectra of the 3 species could be related to partial alignment of the polymer chains. However, the spectra shown were recorded with 100% circularly polarized light which is insensitive to molecular orientation.[41] Several spun cast films were examined using 100% linearly polarized light in several orientations, but there was no evidence of linear dichroic response. We conclude the variations seen among the F 1s spectra plotted in Figure 3 are due to the chemical bonding changes, not to partial alignment.

3.1.3. O 1s Spectra. The O 1s spectra of the Nafion117, Aquivion98, and 3M-725 PFSAs are presented in Figure 4a. Detailed transition assignments are summarized in Table 4. An O 1s spectral signal was also measured from PTFE. Although it should only contain C and F, the very weak O 1s spectrum of PTFE (not shown) was very different from the spectra of PFSA (Figure 4a) and likely arose from residual polymerization catalysts or impurities. The main intensity of the O 1s spectra of PFSA is contained in a broad structure between 535 and 545 eV, which is the region where both O 1s(C−O) → σ^*_{C-O}[48] and O 1s(S−O) → σ^*_{S-O} transitions are expected. This region has a significantly different shape in each of the three species, with that of Aquivion being asymmetric on the high energy side, that of 3M-725 showing signs of a separate peak, and that of Nafion117 having two distinct components, with maxima at 537.0 and 539.6 eV. Nafion117, has two ether (C−O) bonds, whereas the SSC alternatives only have one ether bond. This gives rise to the difference in O 1s NEXAFS observed at both 537 and 540 eV. The difference in intensity at

Table 4. Summary of Peak Positions and Tentative Assignments for Spectral Features in the O 1s Spectra of Nafion117, Aquivion98, and 3M-725

energy (eV)			assignment			
Nafion117	Aquivion98	3M-725	C=O(OR)	COOR	C−O−C	SO_3
531.8[a]	532.2[a]	531.9[a]	$\pi^*_{C=O}$		–	–
535.4 (sh)	535.1 (sh)	535.0 (sh)		$\pi^*_{C=O}$		
537.0	537.5	537.1				σ^*(S−O)
539.6	540.8 (sh)	539.5 (sh)			σ^*(C−O)	
558 (br)	558 (br)	558 (br)				σ^*(S−O)

[a]Calibration: Nafion117: −7.1 (1) eV; Aquivion98: −6.7 (1) eV; 3M-725: −7.0 (1) eV, relative to O 1s → 3s transition of CO_2 (538.9(1) eV[64]).

DOI: 10.1021/acs.jpcc.7b11592
J. Phys. Chem. C XXXX, XXX, XXX−XXX

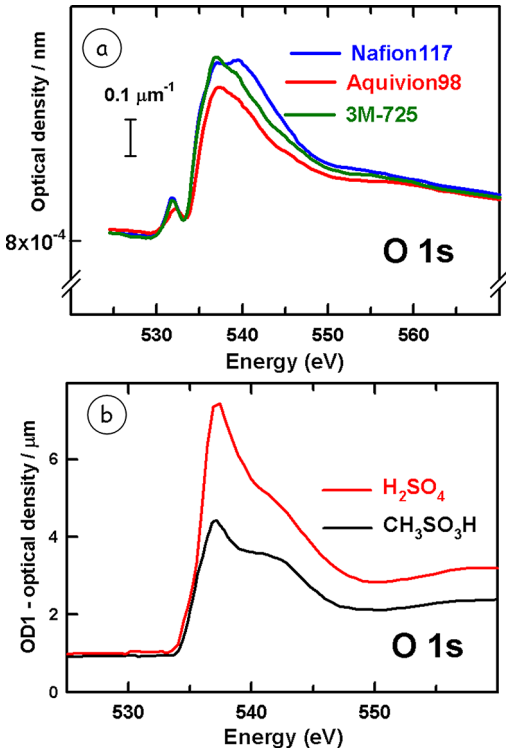

Figure 4. (a) O 1s X-ray absorption spectra of Nafion117, Aquivion98 and 3M-725 recorded using STXM. The spectra have been converted to an absolute intensity scale (optical density/nm thickness at standard density, OD1) using the procedures described in the text. Peak positions and tentative assignments are given in Table 4. (b) O 1s spectra of H_2SO_4 and CH_3SO_3H. The absence of a feature at 532 eV indicates that the prepeak observed in PFSA materials is not due to O 1s → σ^*_{O-H} or O 1s → $\sigma^*_{S=O}$ transitions at the sulfonate group.

~540 eV is introduced by the extra ether bond in the Nafion117 structure. Therefore, the 540 eV transition corresponds to the O 1s → σ^*_{C-O} transition at the ether bond that is closer to the terminal sulfonic acid group. In addition to the broad σ^*_{C-O} signal there is a weak but sharp feature at 532.0 eV. This is the region where O 1s → $\pi^*_{C=O}$ transitions occur. Since PFSA is usually synthesized with the main PTFE chains terminated by carboxylic acid or carboxylate groups,[49,50] it is likely the 532.0 eV feature arises from these end carboxyl groups.

In early studies, we noted a significant difference in the strength of the O 1s pre-edge peak at 532 eV between two different ionomer species (not shown). Initially we attributed the 532 eV peak to O 1s → σ^*_{O-H} transitions at the sulfonic acid group based on a hypothesis suggested from a small molecule core excitation study (see Supporting Information Figure S1). If this was the case, differences in the intensity of this peak would track the differences in degree of protonation of the PFSA, which would be a very useful probe for PEM-FC studies. A peak at 532 eV has been reported in the O 1s NEXAFS spectra of $ZnSO_4$ and ionic liquid antiwear engine additives which have sulfonate groups.[51] In order to test that initial hypothesis we used STXM to measure the O 1s spectra of $H_2SO_4(l)$ and $CH_3SO_3H(l)$ in sealed wet cells (see Figure 4b). Contrary to our expectations based on the initial (and clearly incorrect) spectral interpretation, the O 1s spectra of sulfuric acid and methyl sulfonate do not exhibit a peak at 532 eV, indicating the 532 eV peak observed in PFSA species cannot be due to O 1s → σ^*_{O-H} transitions at the sulfonate group. Rather we assign the 532 eV peak to O 1s → $\pi^*_{C=O}$ transitions at carbonyl groups in the terminal carboxylates. This is consistent with the known energies and relatively sharp peaks for O 1s(C<u>O</u>OR) → $\pi^*_{C=O}$ transitions, and supported by ^{13}C SSNMR (see subsection 3.2.2) as well as our interpretation of the 289 eV peak in the C 1s spectra of the PFSA materials. Unfortunately the 532 eV transition cannot be used as an indication of the degree of protonation of the material.

Another interesting observation related to the 532 eV peak is that this feature is significantly more intense in spin cast films of ionomer dispersions than in microtomed bulk membrane PFSA; see Figure 5a. This could indicate a smaller mean

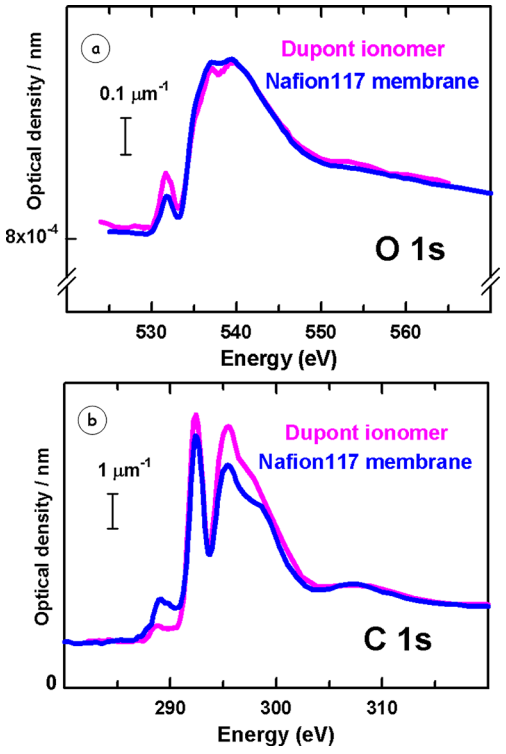

Figure 5. (a) Comparison of O 1s spectra of Dupont ionomer and Nafion117 membrane. (b) Comparison of C 1s spectra of Dupont ionomer and Nafion117 membrane. All spectra were measured in STXM using no-damage defocused beam conditions.

molecular weight, i.e., shorter mean polymer chain, for ionomer (which is expected from the need to solubilize the ionomer in the catalyst ink dispersions) and thus a greater number of carboxylate termination sites relative to ether oxygen side chain sites. However, if that was the case, and our assignment of the 289 eV peak as the corresponding C 1s(C<u>O</u>OX) → $\pi^*_{C=O}$ transition is correct, then the 289 eV peak should be relatively stronger in the ionomer than in the membrane. In fact the opposite is the case; see Figure 5b. In studies of several different types of ionomers, we consistently found these observations (Supporting Information Figure S2). At present, these observations remain a puzzle.

3.1.4. S 2p Spectra. S 2p spectra are sensitive to the local bonding environment of the sulfur[52] and informative in material speciation. The S 2p spectra of the Nafion117, Aquivion98, and 3M-725 PFSAs are presented in Figure 6. Detailed transition assignments are summarized in Table 5. The low lying transition at 172 eV is assigned to overlapping

DOI: 10.1021/acs.jpcc.7b11592
J. Phys. Chem. C XXXX, XXX, XXX−XXX

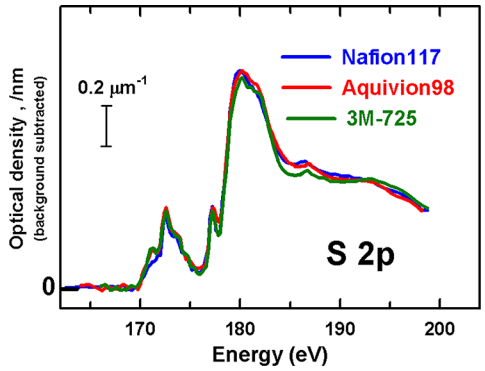

Figure 6. S 2p X-ray absorption spectra of Nafion117, Aquivion98 and 3M-725 recorded using STXM. The as-recorded OD spectra were subjected to a spline fit to generate the nonsulfur background by extrapolating the pre-S 2p signal, which was then subtracted. The intensity scale was then set by matching to similarly background subtracted elemental response functions (OD1-S 2p). Further details are described in the text. Peak positions and tentative assignments are given in Table 5.

S $2p_{3/2,1/2}$ (S−C) → 4s and S $2p_{3/2,1/2}$ (S−O) → 4s transitions which form a characteristic "triplet" structure due to spin−orbital coupling.[53] Transitions in the 178−186 eV region are attributed to spin orbit pairs of S 2p(S−C) → 3d (t_{2g}) and S 2p(S−O) → 3d (t_{2g}) transitions. For all three PFSA materials, the spectral features are very similar, with only slight intensity differences. This is consistent with expectations since the sulfur environments in all three PFSA materials are very similar because the S centers are all in sulfonic acid or sulfonate groups, depending on pH. The only possible change could be due to changes in the degree of protonation of the sulfonate sites, but, as seen from the O 1s edge, a localized σ^*_{S-O-H} orbital either does not exist or the O 1s → σ^*_{S-O-H} and S 2p → σ^*_{S-O-H} transitions are too weak to be detected. The S 2p spectra of these three PFSA materials are similar to the S 2p spectra of gas phase trifluoromethanesulfonate and two other sulfonates, recorded in a complementary inner shell electron energy loss (ISEELS) study (see Supporting Information Figure S3). Since the S 2p spectra of all PFSA samples are identical, we conclude that the sulfonic acid groups in all 3 species have similar local bonding and environments, at least in the dehydrated state. It is important to note that the intensities in Figure 6 do not correlate with the number of sulfonic acid groups present since the spectra have been converted to an optical density per nanometer (OD1) scale which normalizes the S 2p spectra on a per-S basis.

3.2. NMR Spectroscopy. *3.2.1. ^{19}F NMR Spectroscopy.* ^{19}F NMR spectroscopy was performed at ambient temperature and humidity on three PFSA membrane materials after the activation treatment described in the experimental section. With careful deconvolution of the ^{19}F SSNMR signals, each of the different fluorine sites in each PFSA sample are distinguished and assigned, as shown in Figure 7. Peak locations and assignments are summarized in Table 6. The Nafion117 spectrum (Figure 7a) agrees with previous reports.[12] The signal from the side-chain fluorine atoms is well-resolved from those of the backbone. The alternative PFSA materials, Aquivion98 (Figure 7b) and 3M-725 (Figure 7c), have not been studied in detail previously using ^{19}F SSNMR. Importantly, our meticulous deconvolution routine[9,54,55] is an effective tool for distinguishing the molecular structure of the PFSAs. In the spectra of all three PFSAs, the signal at −122 ppm is dominant, and is assigned to the backbone CF_2 moieties, which are the major building blocks of PFSAs. The most noticeable difference of the ^{19}F spectrum of Nafion compared to those of Aquivion98 and 3M-725, is that two -OCF signals observed: one is from the backbone branch point; the other is from that in the side-chain. The OCF_2 signals are found at approximately −80 ppm in all three PFSAs, however the relative signal intensity in Nafion117 is much higher than in the other two PFSAs. This is due to the fact that the signal at −80 ppm in Nafion117 includes contributions from three different fluorine sites, i.e. signal overlap. The SCF_2 site, the terminal fluorine site that is adjacent to the sulfonic acid group, is partially resolved in the spectra. Its signal is very close to that of the backbone CF_2 but the SCF_2 signal intensity can be easily analyzed with deconvolution. Another interesting observation is that the SCF_2 signal in 3M-725 is better resolved than in Nafion117 or Aquivion98. This is possibly caused by the fluorine environment in the material, where the surrounding electronegative fluorines are pulling the electrons more since there are more fluorines nearby in 3M-725. Therefore, the chemical shift of the SCF_2 site is at a relatively higher frequency than the SCF_2 sites in Nafion and Aquivion. Thus, by looking at the general spectral features, these three PFSA materials can be differentiated with sufficient clarity that an unknown material exhibiting one of these three ^{19}F SSNMR spectra could be unambiguously identified.

Table 5. Summary of Peak Positions and Tentative Assignments for Spectral Features in the S 2p Spectra of Nafion117, Aquivion98, and 3M-725

energy (eV)			assignment			
			S−C		SO_3	
Nafion117	Aquivion98	3M-725	$2p_{3/2}$	$2p_{1/2}$	$2p_{3/2}$	$2p_{1/2}$
171.1	171.2	171.1	4s			
172.5[a]	172.6[a]	172.6[a]		4s	4s	
174.1	173.8	174.0				4s
177.3	177.3	177.2	3d (t_{2g})			
178.2 (sh)	179.0 (sh)	178.5		3d (t_{2g})		
180.0	180.2	180.3			3d (t_{2g})	
182.0 (sh)	181.9	182.0				3d (t_{2g})
186.6	186.9	186.8	3d (e_g)	3d (e_g)		
194 (br)	193 (br)	194 (br)			3d (e_g)	3d (e_g)

[a]Calibration: Nafion117: −12.1 eV; Aquivion98: −12.0 eV; 3M-725: −12.0 eV relative to S 2p → t_{2g} transition of SF_6 (184.57(6)[65]).

DOI: 10.1021/acs.jpcc.7b11592
J. Phys. Chem. C XXXX, XXX, XXX−XXX

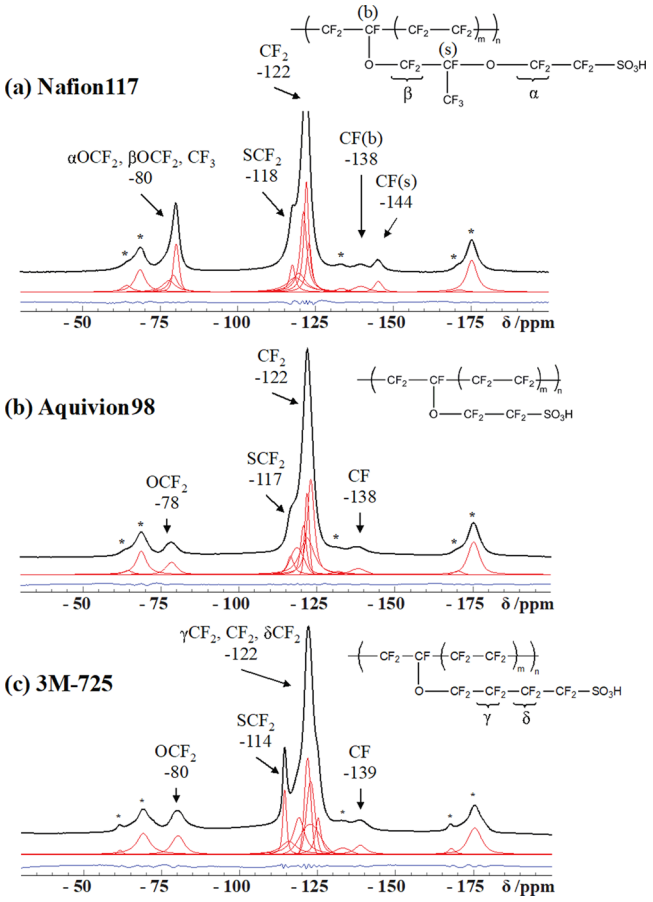

Figure 7. ^{19}F MAS SSNMR of Nafion117, Aquivion98, and 3M-725. The asterisk (*) indicates spinning side bands. Different fluorine sites are labeled accordingly, separating the side chain and backbone signals based on the chemical shifts. Spectral intensities and assignments are given in Table 6.

Quantitative analysis of PFSA composition can also be performed using ^{19}F NMR study. Normalized integrated signal intensities for each fluorine site are summarized in Table 6. The relative intensity ratios agree with the chemical formulas provided by the manufacturers. This indicates that ^{19}F SSNMR can provide quantitative analysis of PFSA materials. ^{19}F SSNMR specifically probes the fluorine environments in PFSA, which can provide unambiguous evidence to identify/distinguish PFSA materials.

3.2.2. ^{13}C NMR Spectroscopy. ^{13}C SSNMR is a challenging experiment due to the low natural abundance of NMR active ^{13}C nucleus. In order to assist transition identification in STXM C 1s NEXAFS analysis, ^{13}C SSNMR spectroscopy was used to identify different carbon environments in three different PFSA materials. The ^{13}C NMR data was collected on materials without ^{13}C enrichment. A field strength of 20 T was used to enhance signal sensitivity. The materials selected were activated Nafion117, and cast film samples from Nafion and Liquion dispersions. It is known that the terminal end group of the polymer chains can be −COOH, $-CF_2H$ or $-CF_2{=}CF_2$ from polymer manufacture.[49,50] A proton decoupling sequence was applied during detection to achieve good signal resolution. All of the carbon sites located on the polymer chains were observed in the chemical shift range 100−120 ppm, shown in Figure 8. The chemical shifts observed agree with the literature for all of the carbon signals expected from the PFSA materials.[55]

In each of the three PFSA samples studied, a carbonyl signal was observed in the ^{13}C SSNMR spectra. These signals have not been reported previously using SSNMR, or any other NMR method, to our knowledge. In Nafion117, this signal occurs at 175.5 ppm (Figure 8a), but in both Nafion and Liquion cast film samples, the carbonyl signals are present at 179 ppm (Figure 8b, c). This chemical shift range has been observed for carbonyl carbons in various materials.[56,57] The variation in chemical shift in these three PFSA materials is possibly due to different cations being associated with the carbonyl groups. The cast films were not prepared in fully protonated form; identification of the cations was not in the scope of this study. Nonetheless, observation of ^{13}C SSNMR signal associated with carbonyl groups in all of the PFSA materials tested is consistent with the literature with regard to the possibility of carboxyl groups as the main chain termination.[49,50] It also supports assignment of the 289 eV NEXAFS peak as the C 1s(COOR)→$\sigma^*_{C=O}$ transition and the 532 eV NEXAFS peak as the O 1s(COOR)→$\sigma^*_{C=O}$ transition at a chain termination carbonyl group.

3.2.3. Diffusion Profile Analysis. The STXM and SSNMR analyses of the ionomer dispersion in cast film form demonstrate the chemical sensitivity of these spectroscopies for identification of different thin films. To further extend this investigation of PFSA cast films starting from different dispersions, the macroscopic diffusion profiles of those dispersions were investigated via NMR spectroscopy. By doing so, the solvated molecular motion can be monitored,

Table 6. Summary of Peak Positions (ppm), Normalized Relative Intensities, and Assignments for Spectral Features in the ^{19}F MAS SSNMR Spectra of Nafion117, Aquivion98, and 3M-725

PFSA		^{19}F SSNMR spectra analysis: chemical shift (ppm) and normalized relative intensity[a]								
Nafion117	type	αOCF_2	βOCF_2	CF_3	SCF_2	CF_2			CF(b)	CF(s)
	δ	−80	−80	−80	−118	−122			−138	−144
	relative intensity	2	2	3	2	28			1	1
Aquivion98	type	OCF2			SCF_2	CF_2			CF	
	δ	−78			−117	−122			−138	
	relative intensity	2			2	30			1	
3M-725	type	OCF2			SCF_2	γCF_2	CF_2	δCF_2	CF	
	δ	−80			−114	−122	−122	−122	−139	
	relative intensity	2			2	2	16	2	1	

[a]Spinning side bands are included in relative intensity normalization.

DOI: 10.1021/acs.jpcc.7b11592
J. Phys. Chem. C XXXX, XXX, XXX−XXX

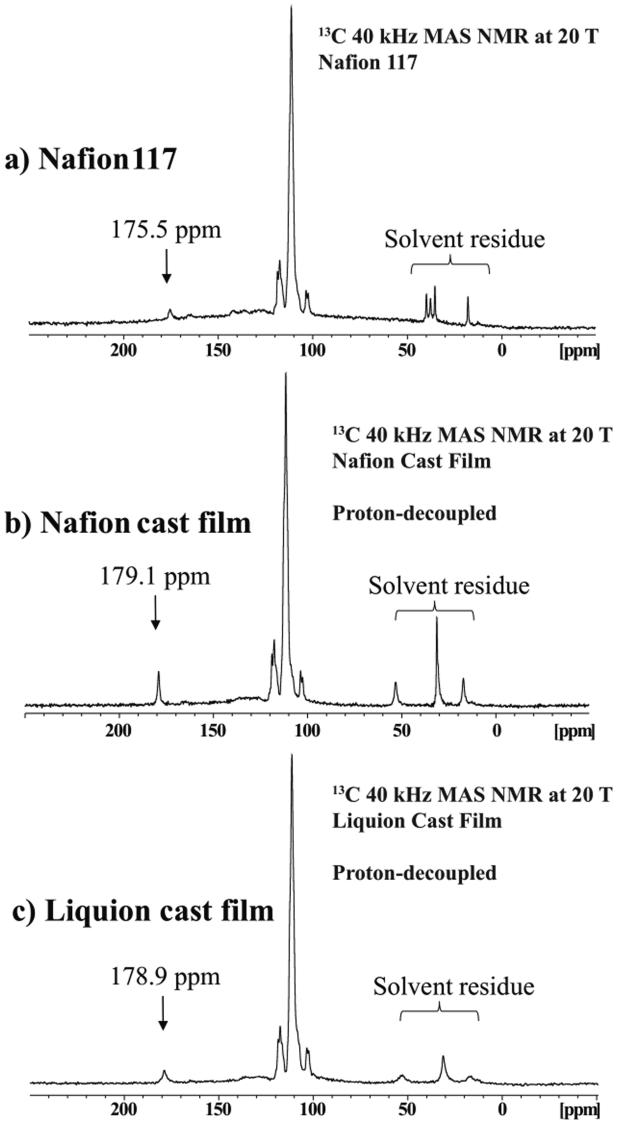

Figure 8. ^{13}C SSNMR of (a) Nafion117, (b) Nafion (EW1100) spin cast film, and (c) Liquion (EW1100) spin cast film.

which provides insight into ionomer film formation in CL and MEA.

Diffusion arises from Brownian motion, where the molecules move randomly in a fluid. It is often characterized by a diffusion coefficient, which is described according to the Stokes−Einstein equation as

$$D = \frac{kT}{6\pi\eta r_s} \tag{1}$$

where k is Boltzmann constant, T is temperature, η is the viscosity of the liquid, and r_s is the radius of the molecule. ^{19}F diffusion ordered NMR spectroscopy (DOSY) experiments for the PFSA dispersions were performed. The pulse sequence used in the current diffusion study can be found in the Supporting Information. The dispersions were obtained from Ion Power Inc. and diluted with *n*-propanol (NPA) aqueous solution with volume ratio NPA/H_2O = 3:1 into 1% concentrated solutions. By doing so, the difference in viscosity in the stock dispersion solutions can be neglected. By monitoring the attenuation of signal intensity, the diffusion coefficient can be extracted by plotting the signal intensity against gradient, according to

$$I = I_0\, e^{-D\gamma^2 g^2 \delta^2 (\Delta - \delta/3)} \tag{2}$$

where D is diffusion coefficient, γ is the gyromagnetic ratio of the observing nucleus, g is the gradient strength, Δ is the diffusion time, and δ is the length of the gradient pulse.

In the current study, the molecular diffusion coefficients were extracted by ^{19}F DOSY experiments at different temperatures, by fitting the signal attenuation trend to the experimental parameters used in the gradient pulse sequence based on the Stejskal and Tanner equation[58] using Bruker Dynamics Center software (v. 2.2.1). The results are plotted in Figure 9. The

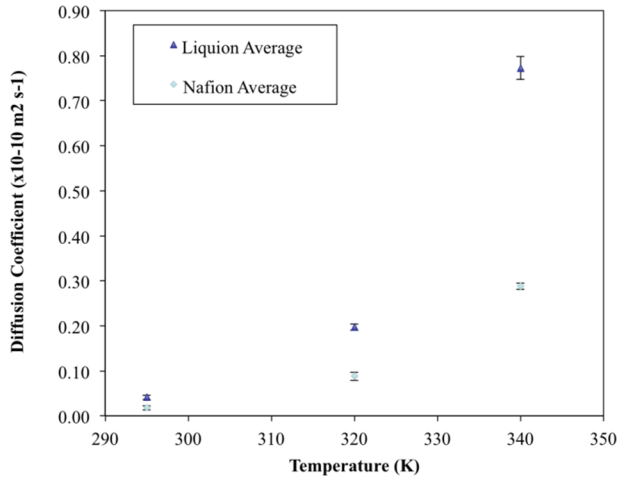

Figure 9. Plot of temperature dependent proton diffusion coefficients in Nafion and Liquion liquid dispersions.

profile diffusion coefficients for different PFSA dispersions were reported by averaging the values for all fluorine sites with 10% difference. The two PFSA dispersions were considered to have the same solution viscosity due to use of the same solvent system, as mentioned previously. In general, the Liquion dispersion has much higher diffusion coefficients at all temperatures, compared to the Nafion dispersion. Taking into account that the two PFSA dispersions were considered to have the same solution viscosity, and the inverse proportionality between the diffusion coefficient and the solvated radius (eq 1), one can conclude that the molecular radius of Liquion dispersion with 1% concentration is smaller than that in a 1% Nafion dispersion. Yet, despite the fact that the chemical compositions of these two dispersions are indistinguishable, the macroscopic diffusion profiles effectively differentiate the two dispersions in terms of solvated molecular radius. ^{19}F diffusion study via NMR spectroscopy is an efficient approach to assist the differentiation of different PFSA ionomer dispersions, and provide self-diffusion profiles of the PFSA molecules.

4. DISCUSSION

This study has explored the strengths and weaknesses of NEXAFS and SSNMR spectroscopies with respect to differentiating PFSA materials in different forms. Together they complement each other from several different perspectives. The STXM technique provides chemical analyses at the C 1s, F 1s, O 1s, and S 2p edges for both membrane and electrode ionomer analysis. From the C 1s and F 1s NEXAFS

DOI: 10.1021/acs.jpcc.7b11592
J. Phys. Chem. C XXXX, XXX, XXX−XXX

investigation, the chemical differentiation was not as clear as we had hoped. Even with detailed transition assignments, the C 1s and F 1s NEXAFS spectra were not able to distinguish PFSA membranes with similar, but differing chemical structures. However, the O 1s NEXAFS was able to differentiate the three PFSA species studied, and thus potentially could be used to identify different PFSA membrane materials. From the O 1s NEXAFS spectral comparison, LSC-PFSA with two ether bonds, like Nafion, can be recognized and separated from the others. In contrast to NEXAFS, ^{19}F NMR analysis provides a powerful way to reveal the complete molecular structures at the fluorine atoms in bulk membrane samples, as demonstrated in Figure 7.

Another form of PFSA, ionomer dispersions, was also explored. The dispersion form is preferred in MEA manufacturing and catalyst layer (CL) casting in the industrial setting due to its tunability, which allows catalyst inks to reach desirable viscosity based on different formulations. When the material form switches from the bulk membrane to the cast thin film made from the ionomer dispersion, such thin films replicate the properties of PFSA materials in fuel cells without the complexity contributed from other MEA or CL components.

The O 1s NEXAFS spectra are sensitive to the chemical bonding between C and O. Spectroscopically, the prepeak at 532 eV is consistent with the presence of terminal carboxylic acid groups,[49,50] an attribution which is supported by ^{13}C NMR. From the NMR perspective, ^{19}F NMR is consistently able to reveal polymeric molecular structure of single-component materials. ^{13}C NMR study at high magnetic field positively identifies the terminal end groups on polymers and speciates residual solvent molecules. The ^{13}C NMR result supports the STXM finding, in that solvent residue signal appears at the lower chemical shift range (10−60 ppm) and carbonyl signal appears at the higher chemical shift range (175−180 ppm). The assignments of the 289 eV C 1s and the 532 eV O 1s signals are still debatable, since these transitions could arise from several possible sources. However, the STXM and NMR results are consistent with each other regarding the existence of carboxyl groups. To further support the NEXAFS peak assignments, additional small molecule investigation could be performed. For example, studies of pentafluoropropionic acid (CF_3CF_2COOH) and its derivatives could help to define the spectra expected for carboxyl groups in a highly fluorinated environment.

By using solution-state NMR with an advanced gradient pulse sequence, the diffusion profiles of the ionomer dispersion were extracted and compared. This demonstrates the power of NMR for combined solid and liquid state studies of PFSA. However, the diffusion experiment performs much more reliably if there are no additional components in the sample system. NMR can easily pick up interfering carbon signals in CL samples, but the existence of paramagnetic catalyst particles causes NMR signal line broadening.

The goal of this research was to explore the relative merits of SSNMR and NEXAFS spectroscopy for characterization of PFSA materials. While SSNMR is clearly more chemically sensitive than NEXAFS, it is not able to investigate the S or O environment directly. NEXAFS requires a synchrotron facility, which is less widely available than lab based solid state NMR. However, if NEXAFS is measured with STXM, spatially resolved chemical mapping can be achieved which benefits investigations of systems with multiple components, such as CL and MEA samples.[12−19] Together, this combination of techniques is able to probe subtle aspects of PFSA materials particularly for studies of degradation as a function of ionomer and membrane composition, following FC operation.[15]

5. SUMMARY

This paper reported an investigation of several different PFSA materials using two spectroscopic techniques, XAS and NMR, which provide different molecular perspectives. NEXAFS spectroscopy via STXM provides chemical sensitivity and spatially resolved (~30 nm) chemical mapping. Together, the C 1s, F 1s, O 1s, and S 2p NEXAFS provide insights into the chemical bonding environment of these elements in PFSAs. S 2p edge studies have great potential to provide insight into selective chemical and electrochemical degradation study of PFSA materials in PEM-FC.[15,59] SSNMR is much more sensitive than NEXAFS in material structure elucidation with qualitative identification and quantitation of different spin environments, since it can detect signals specific to each distinct fluorine site in the repeat unit. However, the natural abundance ^{13}C SSNMR is a "heroic" experiment and ^{33}S SSNMR seems beyond reach of current instrumentation. Within their sensitivity limits, ^{19}F and ^{13}C SSNMR studies can greatly extend STXM analyses of PFSA. Both techniques detected signal from carboxyl groups, which unveils the possible termination of the polymer chain. The existence of carboxyl groups potentially reduces the acidity of the PFSA; however, it may be useful as a chemical stabilizer[49,50] to help ionomer solutions stay dispersed.

STXM analyses of CLs or MEAs can be interpreted with the support of NMR reference data of PFSAs measured without any interference from C support or Pt catalysts, which are essential components in industrial fuel cell devices. At the same time, the S 2p and possibly O 1s NEXAFS can provide localized information on the proton conducting site, the sulfonic acid group, providing another tool to study ionomer materials, even in the presence of other fuel cell CL components. For example, the combination of S 2p NEXAFS and ^{19}F SSNMR would be a powerful approach to study membrane or catalyst layer degradation, or to analyze MEA activation or aging. In particular a STXM-SSNMR combination would have the potential to characterize both the spatial and chemical nature of operationally induced degradation. In particular, attack on PFSA side chains by electrochemically generated free radicals is implicated as a primary damage mechanism during PEM-FC operation.[60] The ability to quantify side-chain loss by high-resolution ^{19}F SSNMR and sulfonic group loss by S 2p XAS would provide a unique vantage point on the degradation process. Furthermore, this approach could be used to evaluate the role of carboxylic acid groups in CL/membrane. Our proclivity is to further utilize STXM to evaluate full CL/MEA components, such that the importance of polymer stability can be probed with spatial resolution.

■ ASSOCIATED CONTENT

Supporting Information

The Supporting Information is available free of charge on the ACS Publications website at DOI: 10.1021/acs.jpcc.7b11592.

NMR pulse sequences and parameters; STXM and ISEELS O 1s spectra and orbital calculations of small molecules; comparison of NEXAFS spectra of microtomed membranes and spun cast films of ionomer

DOI: 10.1021/acs.jpcc.7b11592
J. Phys. Chem. C XXXX, XXX, XXX−XXX

dispersions; STXM and ISEELS S 2p spectra and orbital calculations of small molecules (PDF)

AUTHOR INFORMATION

Corresponding Author

*E-mail: aph@mcmaster.ca.

ORCID

Lis G. A. Melo: 0000-0001-5427-1867

Gillian R. Goward: 0000-0002-7489-3329

Adam P. Hitchcock: 0000-0002-1598-7886

Notes

The authors declare no competing financial interest.

ACKNOWLEDGMENTS

This research was supported by Natural Sciences and Engineering Research Council of Canada – NSERC (Discovery Grants to A.P.H. and G.R.G., CGS/PGS D to Z.B.Y.) and the Automotive Partnership Program CaRPE-FC network, CFI, and the Canada Research Chair program. We thank Dr. S. Krachkovskiy for assistance with the diffusion measurements. We thank 3M (Dr. S. Hamrock) and Solvay S. A. (Dr. L. Merlo) for providing us the cast ionomer materials, and Marcia Reid (Department of Pathology and Molecular Medicine at McMaster University) for expert microtomy sample preparation. Research described in this paper was performed in part at the Canadian Light Source, which is supported by the Canadian Foundation for Innovation, NSERC, the University of Saskatchewan, the Government of Saskatchewan, Western Economic Diversification Canada, the National Research Council Canada, and the Canadian Institutes of Health Research. Results were also acquired at beamline 5.3.2.2 at the ALS, which is supported by the Director of the Office of Science, Department of Energy, under Contract No. DE-AC02-05CH11231.

REFERENCES

(1) Grove, W. R. On Voltaic Series and the Combination of Gases by Platinum. *Philos. Mag.* **1839**, *14*, 127–130.

(2) Perry, M. L.; Fuller, T. F. A Historical Perspective of Fuel Cell Technology in the 20th Century. *J. Electrochem. Soc.* **2002**, *149*, S59–S67.

(3) Holdcroft, S. Fuel Cell Catalyst Layers: A Polymer Science Perspective. *Chem. Mater.* **2014**, *26*, 381–393.

(4) Wang, Y.; Leung, D. Y. C.; Xuan, J.; Wang, H. A Review on Unitized Regenerative Fuel Cell Technologies, Part-A: Unitized Regenerative Proton Exchange Membrane Fuel Cells. *Renewable Sustainable Energy Rev.* **2016**, *65*, 961–977.

(5) Harrop, P. *Fuel Cell Electric Vehicles 2018–2028: Land, Water, Air*; IDTechEx: Boston, 2017.

(6) Gebel, G.; Diat, O. Neutron and X-ray Scattering: Suitable Tools for Studying Ionomer Membranes. *Fuel Cells* **2005**, *5*, 261–276.

(7) Kreuer, K.-D.; Paddison, S. J.; Spohr, E.; Schuster, M. Transport in Proton Conductors for Fuel-Cell Applications: Simulations, Elementary Reactions, and Phenomenology. *Chem. Rev.* **2004**, *104*, 4637–4678.

(8) Mauritz, K. A.; Moore, R. B. State of Understanding of Nafion. *Chem. Rev.* **2004**, *104*, 4535–4586.

(9) Ghassemzadeh, L.; Kreuer, K. D.; Maier, J.; Müller, K. Evaluating Chemical Degradation of Proton Conducting Perfluorosulfonic Acid Ionomer in a Fenton Test by Solid-state ^{19}F NMR Spectroscopy. *J. Power Sources* **2011**, *196*, 2490–2497.

(10) Ghassemzadeh, L.; Holdcroft, S. Quantifying the Structural Changes of Perfluorosulfonated Acid Ionomer upon Reaction with Hydroxyl Radicals. *J. Am. Chem. Soc.* **2013**, *135*, 8181–8184.

(11) Lepiller, C.; Gauthier, V.; Gaudet, J.; Pereira, A.; Lefevre, M.; Guay, D.; Hitchcock, A. P. Studies of Nafion® - $RuO_2.xH_2O$ Composite Membranes. *J. Electrochem. Soc.* **2008**, *155*, B70–B78.

(12) Susac, D.; Berejnov, V.; Hitchcock, A. P.; Stumper, J. STXM Study of the Ionomer Distribution in PEM Fuel Cell Catalyst Layers. *ECS Trans.* **2011**, *41*, 629–635.

(13) Berejnov, V.; Susac, D.; Stumper, J.; Hitchcock, A. P. 3D Chemical Mapping of PEM Fuel Cell Cathodes by Scanning Transmission Soft X-ray Spectrotomography. *ECS Trans.* **2013**, *50*, 361–368.

(14) Susac, D.; Berejnov, V.; Hitchcock, A. P.; Stumper, J. STXM Characterization of PEM Fuel Cell Catalyst Layers. *ECS Trans.* **2013**, *50*, 405–413.

(15) Hitchcock, A. P.; Berejnov, V.; Lee, V.; West, M. M.; Dutta, M.; Colbow, V.; Wessel, S. Carbon corrosion of Proton Exchange Membrane Fuel Cell catalyst layers studied by Scanning Transmission X-ray Microscopy. *J. Power Sources* **2014**, *266*, 66–78.

(16) Lee, V.; Berejnov, V.; West, M. M.; Kundu, S.; Susac, D.; Stumper, J.; Atanasoski, R. T.; Debe, M.; Hitchcock, A. P. STXM Investigations of Nano Structured Thin Film Catalysts for Proton-Exchange-Membrane Fuel Cell Applications. *J. Power Sources* **2014**, *263*, 163–174.

(17) Hitchcock, A. P.; Wu, J.; Lee, V.; Appathurai, N.; Tyliszczak, T.; Shiu, H.-W.; Shapiro, D.; Berejnov, V.; Susac, D.; Stumper, J. Progress in soft X-ray Microscopy Characterization of PEM Fuel Cell Catalyst Layers. *Microsc. Microanal.* **2016**, *22*, 1290–1291.

(18) Berejnov, V.; Saha, M. S.; Susac, D.; Stumper, J.; West, M. M.; Hitchcock, A. P. Advances in Structural Characterization Using Soft X-ray Scanning Transmission Microscopy (STXM): Mapping and Measuring Porosity in PEM-FC Catalyst Layers. *ECS Trans.* **2017**, *80*, 241–252.

(19) G. A. Melo, L.; Hitchcock, A. P.; Jankovic, J.; Susac, D.; Stumper, J.; Berejnov, V. Quantitative mapping of PFSA Ionomer in Catalyst Layers by Electron and X-ray Spectromicroscopy. *ECS Trans.* **2017**, *80*, 275–282.

(20) Yakovlev, S.; Balsara, N. P.; Downing, K. H. Insights on the Study of Nafion® Nanoscale Morphology by Transmission Electron Microscopy. *Membranes* **2013**, *3*, 424–439.

(21) Wang, C.; Duscher, G.; Paddison, S. J. Characterization of Chain Conformations in Perfluorosulfonic Acid Membranes Using Electron Energy Loss Spectroscopy. *RSC Adv.* **2015**, *5*, 2368–2373.

(22) Rightor, E. G.; Hitchcock, A. P.; Ade, H.; Leapman, R. D.; Urquhart, S. G.; Smith, A. P.; Mitchell, G.; Fischer, D.; Shin, H. J.; Warwick, T. Spectromicroscopy of poly(ethylene terephthalate): Comparison of Spectra and Radiation Damage Rates in X-ray Absorption and Electron Energy Loss. *J. Phys. Chem. B* **1997**, *101*, 1950–1960.

(23) Wang, J.; Botton, G. A.; West, M. M.; Hitchcock, A. P. Quantitative Evaluation of Radiation Damage to Polyethylene Terephthalate by Soft X-rays and High-energy Electrons. *J. Phys. Chem. B* **2009**, *113*, 1869–1876.

(24) de A. Melo, L. G.; Botton, G. A.; Hitchcock, A. P. Quantification of the Critical Dose for Radiation Damage to Perfluorosulfonic Acid Membranes Using Soft X-ray Microscopy. *Microsc. Microanal.* **2015**, *21*, 2443–2444.

(25) Levitt, M. H. *Spin dynamics: basics of nuclear magnetic resonance*; John Wiley & Sons: Chichester, UK, 2001.

(26) Duer, M. J. *Introduction to Solid-state NMR Spectroscopy*; Blackwell Science: Oxford, UK, 2004.

(27) Hitchcock, A. P. Soft X-ray spectromicroscopy and ptychography. *J. Electron Spectrosc. Relat. Phenom.* **2015**, *200*, 49–63.

(28) Hitchcock, A. P.; Lee, V.; Wu, J.; West, M. M.; Cooper, G.; Berejnov, V.; Soboleva, T.; Susac, D.; Stumper, J. Characterizing Automotive Fuel Cell Materials by Soft X-Ray Scanning Transmission X-Ray Microscopy. *AIP Conf. Proc.* **2014**, *1696*, 020012.

(29) Cody, G. D.; Heying, E.; Alexander, C. M. O.; Nittler, L. R.; Kilcoyne, A. L. D.; Sandford, S. A.; Stroud, R. M. Establishing a Molecular Relationship between Chondritic and Cometary Organic Solids. *Proc. Natl. Acad. Sci. U. S. A.* **2011**, *108*, 19171–19176.

DOI: 10.1021/acs.jpcc.7b11592
J. Phys. Chem. C XXXX, XXX, XXX–XXX

(30) Maia, L. J. Q.; Mastelaro, V. R.; Schneider, J. F.; Parent, P.; Laffon, C. Structual Studies in the $BaO-B_2O_3-TiO_2$ System by XAFS and ^{11}B-NMR. *J. Solid State Chem.* **2005**, *178*, 1452−1463.
(31) Vigolo, M.; Borsacchi, S.; Sorarù, A.; Geppi, M.; Smarsly, B. M.; Dolcet, P.; Rizzato, S.; Carraro, M.; Gross, S. Engineering of Oxoclusters-Reinforced Polymeric Materials with Application as Heterogeneous Oxydesulfurization Catalysts. *Appl. Catal., B* **2016**, *182*, 636−644.
(32) Hamrock, S. J.; Yandrasits, M. A. Proton Exchange Membranes for Fuel Cell Applications. *J. Macromol. Sci., Polym. Rev.* **2006**, *46*, 219−244.
(33) Kilcoyne, A. L. D.; Tyliszczak, T.; Steele, W. F.; Fakra, S.; Hitchcock, P.; Franck, K.; Anderson, E.; Harteneck, B.; Rightor, E. G.; Mitchell, G. E.; Hitchcock, A. P.; Yang, L.; Ade, H. Interferometer-Controlled Scanning Transmission X-ray Microscopes at the Advanced Light Source. *J. Synchrotron Radiat.* **2003**, *10*, 125−136.
(34) Warwick, T.; Ade, H.; Kilcoyne, D.; Kritscher, M.; Tylisczcak, T.; Fakra, S.; Hitchcock, A. P.; Hitchcock, P.; Padmore, H. A New Bend Magnet Beam Line for Scanning Transmission X-ray Microscopy at the Advanced Light Source. *J. Synchrotron Radiat.* **2002**, *9*, 254−257.
(35) Kaznatcheev, K. V.; Karunakaran, C.; Lanke, U. D.; Urquhart, S. G.; Obst, M.; Hitchcock, A. P. Soft X-ray Spectromicroscopy Beamline at the CLS: Commissioning Results. *Nucl. Instrum. Methods Phys. Res., Sect. A* **2007**, *582*, 96−99.
(36) Ade, H.; Hitchcock, A. P. NEXAFS Microscopy and Resonant Scattering: Composition and Orientation Probed in Real and Reciprocal Space. *Polymer* **2008**, *49*, 643−675.
(37) Hitchcock, A. P. In *Handbook on Nanoscopy*; Van Tendeloo, G., Van Dyck, D., Pennycook, S. J., Eds.; Wiley: New York, 2012; Vol. *II*, Chapter 22, pp 745−791.
(38) Jacobsen, C.; Wirick, S.; Flynn, G.; Zimba, C. Soft X-ray Spectroscopy from Image Sequences with Sub-100 nm Spatial Resolution. *J. Microsc.* **2000**, *197*, 173−184.
(39) Henke, B. L.; Gullikson, E. M.; Davis, J. C. X-Ray Interactions: Photoabsorption, Scattering, Transmission, and Reflection at E = 50−30,000 eV, Z = 1−92. *At. Data Nucl. Data Tables* **1993**, *54*, 181−342.
(40) Hitchcock, A. P. aXis2000 is written in Interactive Data Language (IDL). It is available free for non-commercial use fromhttp://unicorn.mcmaster.ca/aXis2000.html. Accessed November 15, 2017.
(41) Stöhr, J. *NEXAFS Spectroscopy*; Springer: Berlin, Germany, 1992.
(42) Ishii, I.; McLaren, R.; Hitchcock, A. P.; Jordan, K. D.; Choi, H.; Robin, M. B. The σ^* Molecular Orbitals of Perfluoroalkanes as Studied by Inner Shell Electron Energy Loss and Electron Transmission Spectroscopies. *Can. J. Chem.* **1988**, *66*, 2104−2121.
(43) Robin, M. B.; Ishii, I.; McLaren, R.; Hitchcock, A. P. Fluorination Effects on the Inner-shell Spectra of Unsaturated Molecules. *J. Electron Spectrosc. Relat. Phenom.* **1988**, *47*, 53−92.
(44) Ohta, T.; Seki, K.; Yokoyama, T.; Morisada, I.; Edamatsu, K. Polarized XANES Studies of Oriented Polyethylene and Fluorinated Polyethylenes. *Phys. Scr.* **1990**, *41*, 150−153.
(45) Castner, D. G.; Lewis, K. B., Jr; Fischer, D. A.; Ratner, B. D.; Gland, J. L. Determination of Surface Structure and Orientation of Polymerized Tetrafluoroethylene Films by Near-Edge X-ray Absorption Fine Structure, X-ray Photoelectron Spectroscopy, and Static Secondary Ion Mass Spectrometry. *Langmuir* **1993**, *9*, 537−542.
(46) Ziegler, C.; Schedel-Niedrig, T.; Beamson, G.; Clark, D. T.; Salaneck, W. R.; Sotobayashi, H.; Bradshaw, A. M. X-ray Absorption Study of Highly Oriented Poly(tetrafluoroethy1ene) Thin Films. *Langmuir* **1994**, *10*, 4399−4402.
(47) Sette, F.; Stöhr, J.; Hitchcock, A. P. Determination of Intra-Molecular Bond Lengths in Gas Phase Molecules from K-Shell Shape Resonances. *J. Chem. Phys.* **1984**, *81*, 4906−4914.
(48) Urquhart, S. G.; Hitchcock, A. P.; Priester, R. D.; Rightor, E. G. Analysis of Polyurethanes using Core Excitation Spectroscopy. Part II. Inner-shell Spectra of Ether, Urea and Carbamate Model Compounds. *J. Polym. Sci., Part B: Polym. Phys.* **1995**, *33*, 1603−1620.
(49) Curtin, D. E.; Lousenberg, R. D.; Henry, T. J.; Tangeman, P. C.; Tisack, M. E. Advanced Materials for Improved PEM-FC Performance and Life. *J. Power Sources* **2004**, *131*, 41−48.
(50) Yu, T. H.; Liu, W.-G.; Sha, Y.; Merinov, B.; Shirvanian, P.; Goddard, W. A., III The Effect of Different Environments on Nafion® Degradation: Quantum Mechanics Study. *J. Membr. Sci.* **2013**, *437*, 276−285.
(51) Sharma, V.; Gabler, C.; Doerr, N.; Aswath, P. B. Mechanism of Tribofilm Formation with P and S Containing Ionic Liquids. *Tribol. Int.* **2015**, *92*, 353−364.
(52) Hay, S. J.; Metson, J. B.; Hyland, M. M. Sulfur Speciation in Aluminum Smelting Anodes. *Ind. Eng. Chem. Res.* **2004**, *43*, 1690−1700.
(53) Bernini, R. B.; da Silva, L. B. G.; Rodrigues, F. N.; Coutinho, L. H.; Rocha, A. B.; de Souza, G. G. B. Core Level (S 2p) Excitation and Fragmentation of the Dimethyl Sulfide and Dimethyldisulfide Molecules. *J. Chem. Phys.* **2012**, *136*, 144307.
(54) Yan, Z. B.; Brouwer, D. H.; Goward, G. R. ^{19}F Double Quantum NMR Spectroscopy: A Tool for Probing Dynamics in Proton-Conducting Fluorinated Polymer Materials,. *Macromolecules* **2016**, *49*, 7331−7339.
(55) Chen, Q.; Schmidt-Rohr, K. ^{19}F and ^{13}C NMR Signal Assignment and Analysis in a Perfluorinated Ionomer (Nafion) by Two-Dimensional Solid-State NMR. *Macromolecules* **2004**, *37*, 5995−6003.
(56) Spera, S.; Bax, A. Empirical Correlation between Protein Backbone Conformation and Cα and Cβ ^{13}C Nuclear Magnetic Resonance Chemical Shifts. *J. Am. Chem. Soc.* **1991**, *113*, 5490−5492.
(57) Wishart, D. S.; Bigam, C. G.; Holm, A.; Hodges, R. S.; Sykes, B. D. ^{1}H, ^{13}C and ^{15}N Random Coil NMR Chemical Shifts of the Common Amino Acids. I. Investigations of Nearest-Neighbor Effects. *J. Biomol. NMR* **1995**, *5*, 67−81.
(58) Stejskal, E. O.; Tanner, J. E. Spin Diffusion Measurements: Spin Echoes in the Presence of a Time-Dependent Field Gradient. *J. Chem. Phys.* **1965**, *42*, 288−292.
(59) de A. Melo, L. G.; West, M. M.; Berejnov, V.; Hitchcock, A. P. X-ray Damage of Perfluorosulfonic acid, Polytetrafluoroethylene and Teflon-AF Studied by Scanning Transmission X-ray Microscopy. Manuscript in preparation, 2018.
(60) Coms, F. D. The Chemistry of Fuel Cell Membrane Chemical Degradation. *J. Electrochem. Soc. Trans.* **2008**, *16*, 235−255.
(61) Moukheiber, E.; De Moor, G.; Flandin, L.; Bas, C. Investigation of ionomer structure through its dependence on ion exchange capacity (IEC). *J. Membr. Sci.* **2012**, *389*, 294−304.
(62) Ma, Y.; Chen, C. T.; Meigs, G.; Randall, K.; Sette, F. High-Resolution K-shell photoabsorption measurements of simple molecules. *Phys. Rev. A: At., Mol., Opt. Phys.* **1991**, *44*, 1848−1858.
(63) Sodhi, R. N. S.; Brion, C. E. Reference Energy for Inner Shell Electron Energy-Loss Spectroscopy. *J. Electron Spectrosc. Relat. Phenom.* **1984**, *34*, 363−372.
(64) Hitchcock, A. P.; Ishii, I. Carbon K-shell Excitation Spectra of Linear and Branched Alkanes. *J. Electron Spectrosc. Relat. Phenom.* **1987**, *42*, 11−26.
(65) Hudson, E.; Shirley, D. A.; Domke, M.; Remmers, G.; Puschmann, A.; Mandel, T.; Xue, C.; Kaindl, G. High-Resolution Measurements of Near-Edge Resonances in the Core-Level Photoionization Spectra of SF_6. *Phys. Rev. A: At., Mol., Opt. Phys.* **1993**, *47*, 361−373.

DOI: 10.1021/acs.jpcc.7b11592
J. Phys. Chem. C XXXX, XXX, XXX−XXX